Published in International Journal of Quantum Chemistry 101: 753–760, 2005

# DFT Study of Mixed-Valent Mn(II/III) Hexacyanide Clusters

**CLAUDE DAUL, CÉDRICK RAUZY, SILVIO DECURTINS, PATRICK FRANZ, ANDREAS HAUSER**

[1] *Département de Chimie, Université de Fribourg–Pérolles, CH-1700 Fribourg, Switzerland*

[2] *Department of Chemistry and Biochemistry, University of Bern, Bern, Switzerland*

[3] *Département de Chimie Physique, Université de Genève, Genève, Switzerland*

*Received 18 September 2003; accepted 19 January 2004*
*Published online 1 November 2004 in Wiley InterScience (www.interscience.wiley.com).*
*DOI 10.1002/qua.20333*

**ABSTRACT:** The cubic Prussian blue analogue $Mn_3[Mn(CN)_6]_2 \cdot 15\ H_2O$, which has the advantage of being transparent and magnetic ($T_N$ = 35 K) at the same time, has been investigated by density functional theory (DFT) calculations. The three-dimensional structure is built of $Mn^{II}$ ions linked to $Mn^{III}$ ions by $\mu$-bridging cyanides, to form a crystal structure, which is related to the NaCl type. In a first step, the relative stabilities of the mononuclear complexes $[Mn(CN)_6]^{z-}$ ($z$ = 2 to 4) have been studied as a function of the oxidation state, spin configuration, and the linkage isomerism of the cyanide ligand. The results we have obtained by this investigation are in good agreement with our chemical expertise. In addition, the calculations have been extended to the dinuclear $[Mn_2(CN)_{11}]^{z-}$ ($z$ = 5 and 6) clusters. Furthermore, we used DFT to model the magnetic properties as well as the $^3T_1 \rightarrow {}^1T_2$ transition, which has been observed by single-crystal near-IR spectra of $Mn_3[Mn(CN)_6]_2 \cdot 15\ H_2O$.

**Key words:** cluster; cyanide bridging ligand; DFT; manganese complexes; Prussian blue analogue

## Introduction

Transition metal cyanide chemistry on the one hand has a remarkable history [1] and on the other hand shows a revival, offering exciting prospects in the field of materials chemistry. The systematic investigation of Prussian blue (PB) and its analogues was started in the 1970s by Buser et al. [2]. The potential of the $\mu$-bridging cyanides to act as very efficient mediators of strong magnetic coupling between transition metal ions convinced many chemists to work in the field of PB analogues. Currently, research efforts are focused on the development of PB analogue materials bearing paramagnetic metal centers, which exhibit spontaneous

*Correspondence to:* C. Rauzy; e-mail: cedrick.rauzy@unifr.ch
Contract grant sponsor: Swiss National Science Foundation.
Contract grant number: NRP47

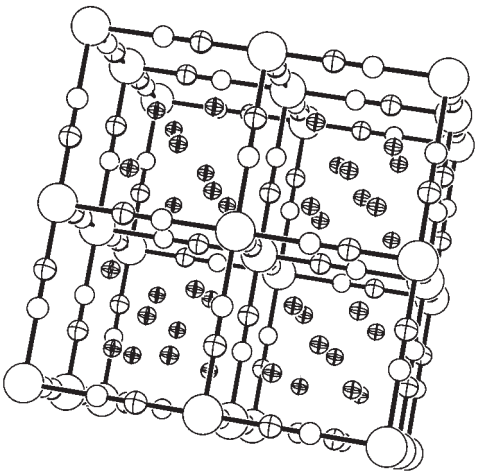

**FIGURE 1.** The PB network of $Mn_3[Mn(CN)_6]_2 \cdot 15$ $H_2O$, a cubic, face-centered crystal.

magnetization at comparatively high temperature. Recent milestones in these efforts are based on the discovery of a room-temperature magnetic PB phase [3, 4] as well as on the first molecule-based magnet, which retains magnetization up to 400 K [5]. It could also been shown that magnetic properties with electrochemical and optical stimuli can also be combined in PB analogues [6, 7]. However, despite this substantial progress, a major drawback is the air-sensitive and amorphous character of most of the PB compounds.

In this study, we present a computational investigation of an air-stable PB, which can easily be prepared in the form of single crystals with a face-centered cubic structure and which exhibit transparency, color, and a ferrimagnetic phase (the structural picture of the compound is given in Fig. 1). Two approaches to model this compound are feasible: a band structure calculation and a model cluster approach. The latter one was chosen, and we used density functional theory (DFT), applying it first to $[Mn(CN)_6]^{z-}$ (for $z = 2$, 3, and 4) units and second to the dimer units $[Mn_2(CN)_{11}]^{z-}$ (for $z = 5$ and 6), which are mixed valent and used to model the properties of the compound drawn in Figure 1. Therefore, a detailed investigation of the $[Mn(CN)_6]^{z-}$ unit with bond length and angles based on X-ray crystallographic data was started. As a result, relative stabilities were obtained as a function of the oxidation state, the spin configuration (high-spin/low-spin), and linkage isomerism of the cyanide ligands. In a second step, the calculations were extended to the dimeric dinuclear $[Mn_2(CN)_{11}]^{z-}$ clusters. Moreover, the $^3T_1 \rightarrow {}^1T_2$ transition of a $Mn^{III}$ ion in low-spin configuration, which could be observed by single-crystal near-IR spectroscopy, could be simulated by DFT, in good agreement with the experimental data.

## Computational Details

The DFT calculations were performed with the Amsterdam Density Functional (ADF) program package (release 2000.02) [8]. For exchange-correlation functionals, the generalized gradient approximation (GGA) has been used. However, all numerical data presented in this article refer to the GGA approximation and are expressed in eV. The local density approximation (LDA) was applied using the X$\alpha$ functional for the exchange ($\alpha = 0.7$) [9] and the Vosko, Wilk, and Nusair functional for the correlation [10]. The GGA was applied using the exchange and correlation proposed by Perdew and Wang [11]. The frozen-core approximation was used for the inner-core electrons. The orbitals up to 2p for manganese and 1s for nitrogen and carbon were kept frozen. The valence shells were described by a triple-$\zeta$ Slater-type orbital (STO) set plus one polarization function.

All calculations were performed as single-point calculations. In fact, the complexes or clusters studied in this article are highly negative, and we had to add positive point charges to act as counterbalance. This prohibited the ADF package from performing geometry optimizations. For the mononuclear complexes, the default self-consistent field (SCF) parameters of ADF were used (DIIS [15–17] [direct inversion of the iterative subspace] activate, mixing ratio equal to 0.2, integration [12, 13] equal to 4.0 and convergence criteria fixed to $1 \cdot 10_6$). For the dinuclear cluster, the DIIS had to be deactivated, the numerical integration increased to 8.0 (to account for the presence of two metallic cations with almost the same environment), and the mixing ratio had to be reduced to 0.02. The strategy was first to run single point calculations using the *xyz* parameters from X-ray crystallography and the desired charges by applying the restricted formalism. After analyzing the first output (file resulting from a calculation) and determining molecular orbital, which is composed of atomic *d*-orbitals of cations, we ran single-point calculations with fixed molecular orbital (MO) occupations applying the spin-unrestricted formalism. For this second set of calculations, SCF parameters used were the same as those

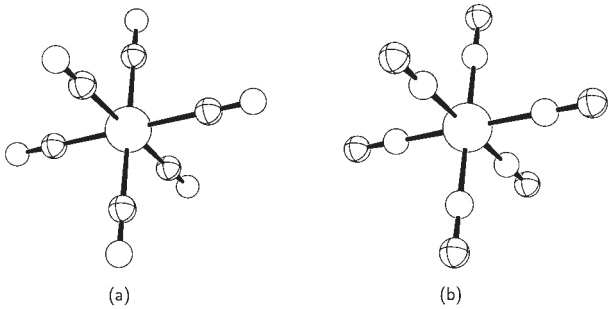


**FIGURE 2.** The two $[Mn(CN)_6]^{z-}$ mononuclear complexes studied by DFT with the cyanide ligand C-coordinated (a) and N-coordinated (b).

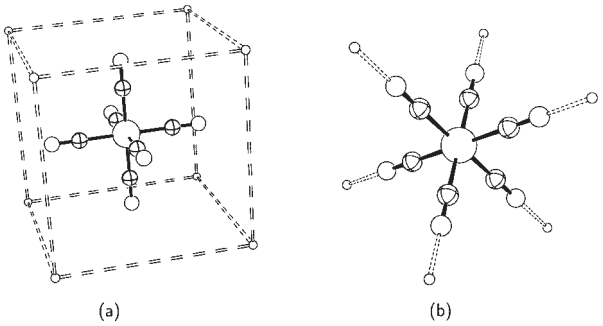


**FIGURE 3.** The two sets of point charge positions, corresponding to (a) cubic and (b) ligand positions. We used this nomenclature throughout.

described previously. As before, the density was allowed to relax according to the desired occupation.

## Results and Discussions

### INVESTIGATION OF THE MONONUCLEAR SPECIES: $[MN(CN)_6]^{Z-}$

Three aspects for the investigation of the $[Mn(CN)_6]^{z-}$ had to be considered. First of all, the manganese ion can exist in several oxidation states, namely, II ($d^5$), III ($d^4$), and IV ($d^3$). Second, the electronic configuration with respect to high-spin (HS) and low-spin (LS) can be distinguished for the $d^5$ and $d^4$ configurations. At last, the cyanide ligand has an ambidentate nature. It can therefore be linked to the metal ion by the carbon or the nitrogen atom.

As a result, 10 calculations had to be performed: four cases for C-coordinated $Mn^{II}$ and $Mn^{III}$ in HS and LS states and one for C-coordinated $Mn^{IV}$ and the same for the N-coordinated cyanide ligand (Fig. 2).

Due to the fact that the complexes are highly negatively charged, simple DFT calculations result in electronic occupation of MOs at positive eigenvalues. One way to avoid this problem is to put positive point charges around the octahedral complex. This approach was performed in two ways. First, the positive charges were placed along the axis of the ligands (called "ligand position") and secondly, they were situated at the corners of a cube around the octahedral complex (called "cubic position") (Fig. 3).

All studies were performed as single-point calculations without geometry optimizations. The bond lengths used for the calculations are based on X-ray investigations. However, the nitrogen and the carbon atoms can hardly be distinguished by X-ray analysis, because they have a similar number of electrons. Therefore, two geometries were investigated where the cyanide bridge was inverted (interchange of the Mn–C and Mn–N bond length) (Table I).

In this report the $[Mn(CN)_6]^{z-}$ investigation has two parts. First, the influence of the positive point charges was studied, and second, the calculations according to the geometries defined in Table I were performed.

#### Influence of Point-Charge Positions for Geometry 1

As mentioned above, due to the high negative charges of the $[Mn(CN)_6]^{z-}$ complexes, MOs with

**TABLE I**

**The two sets of coordinates investigated for the mononuclear complex $[Mn(CN)_6]^{z-}$.[a]**

| Geometry 1 | | Geometry 2 | |
|---|---|---|---|
| N-coordinated | C-coordinated | N-coordinated | C-coordinated |
| $d_{Mn-N}$ = 2.1886 Å<br>$d_{N-C}$ = 1.1458 Å | $d_{Mn-C}$ = 1.9751 Å<br>$d_{C-N}$ = 1.1458 Å | $d_{Mn-N}$ = 1.9751 Å<br>$d_{N-C}$ = 1.1458 Å | $d_{Mn-C}$ = 2.1886 Å<br>$d_{C-N}$ = 1.1458 Å |

[a]Geometry 1 is more in agreement with our chemical intuition; nevertheless, we investigate the two possibilities.

**TABLE II**

**The complete set of energy calculations [eV] for the complex $[Mn(CN)_6]^{z-}$ for geometry 1 (see Table I).[a]**

| | | $[Mn(CN)_6]^{-4}$ $Mn^{II}$ ($d^5$) | | $[Mn(CN)_6]^{-3}$ $Mn^{III}$ ($d^4$) | | $[Mn(CN)_6]^{-2}$ |
|---|---|---|---|---|---|---|
| | | HS | LS | HS | LS | $Mn^{IV}$ ($d^3$) |
| N-coordinated | Cubic | **−156.78** | −155.90 | **−150.24** | −149.79 | −138.91 |
| | Ligand | **−151.50** | −150.56 | **−146.86** | −146.38 | −137.32 |
| C-coordinated | Cubic | −154.18 | **−159.65** | −151.67 | **−154.36** | −144.04 |
| | Ligand | −146.56 | **−151.96** | −146.41 | **−149.09** | −141.21 |

[a] The ligand and cubic notation refer to the point charge position around the complex according to Figure 3.

positive eigenvalues were initially occupied in the DFT calculations. This could be overcome by adding positive point charges to balance the excess of the negative charges of the cyanide ligand. To check the influence of the positions of the positive point charges, two possibilities were taken into account. The first one is with the positive charges on the corners of a cube surrounding the complex [Fig. 3(a)] and the second, with the point charges situated on the ligand axis [Fig. 3(b)]. The numerical results are given in Table II. The difference between the HS and LS configuration was then compared and summarized (Table III). Depending on the positions of the point charges, the energies of the MOs shift. By building the difference of the HS and the LS configuration, the shift in the energies is canceled out, and the influence of the point charges can be compared. Because the energy differences of HS and LS of the two possibilities in Table III are very similar, we can conclude that there is no influence on the results in which we are interested. Therefore, in the rest of the current paper, only the so-called "ligand" point-charge position is taken into account.

## Influence of Bond Length

*Geometry 1.* The geometry of $[Mn(CN)_6]^{z-}$ is perfectly octahedral, and the cyanide-to-metal bond does not deviate from linearity. According to the discussion above, Table II can be reduced to Table IV, and the lower energies are emphasized by bold letters. The manganese ion in N-coordination is lower in energy in HS configuration, whereas the manganese ion in C-coordinations is lower in energy in LS configuration. It should be stressed that only the energies for the same number of electrons (same oxidation state) can be compared. This outcome is consistent with our knowledge of the influence of the *d*-electron configuration on the ligand field splitting and the spectrochemical series.

*Geometry 2.* Due to the difficulties to distinguish between carbon and nitrogen in X-ray spectroscopy, the cyanide was turned around, such that the Mn–C bond is longer than the Mn–N bond (Table I). The energies of this configuration for the point charges in the ligand positions are summarized in Table V. At this point, two conclusions can be drawn: first, all energies for the LS configuration are more stable than for the HS configuration; and,

**TABLE III**

**According to the values of Table II, we compare the difference between high- and low-spin energies.[a]**

| | | $d^5$ $E_{(high\ spin)} - E_{(low\ spin)}$ | $d^4$ $E_{(high\ spin)} - E_{(low\ spin)}$ | $d^3$ |
|---|---|---|---|---|
| N-coordinated | Cubic | −0.88 | −0.45 | −138.91 |
| | Ligand | −0.94 | −0.48 | −137.32 |
| C-coordinated | Cubic | 5.47 | 2.69 | −144.04 |
| | Ligand | 5.40 | 2.68 | −141.21 |

[a] By this, we avoid any shifting process. We can see that for $d^4$, the energy between the two point-charge positions are so close that we can arrive at the conclusion that point-charge positions have no influence on the result (energies are given in eV).

**TABLE IV**

**Following the reasoning exposed in the section titled "Investigation of the Mononuclear Species: $[Mn(CN)_6]^{z-}$," we reduce Table II to this one.[a]**

| | $[Mn(CN)_6]^{-4}$ $Mn^{II}$ ($d^5$) | | $[Mn(CN)_6]^{-3}$ $Mn^{III}$ ($d^4$) | | $[Mn(CN)_6]^{-2}$ $Mn^{IV}$ ($d^3$) |
|---|---|---|---|---|---|
| | HS | LS | HS | LS | |
| CN link by N | **−151.50** | −150.56 | **−146.86** | −146.38 | −137.32 |
| CN link by C | −146.56 | **−151.96** | −146.41 | **−149.09** | −141.21 |

[a] Bold fonts underline the most stable configuration between HS and LS configuration.

second, the energies for this case are higher than those for geometry 1. Therefore, geometry 1 is more stable by 5 to 10 eV.

By this set of calculations, we could demonstrate that DFT confirmed our chemical experience that the geometry with the shorter Mn–C bond and the longer Mn–N bond is favored.

## INVESTIGATION OF THE DINUCLEAR SPECIES: $[Mn_2(CN)_{11}]^{z-}$

In a next step, the calculations were extended to dinuclear clusters. According to the knowledge we gained from the previous calculations, it was sufficient to calculate only the equivalent to geometry 1 with the positive point charges in the ligand positions (Fig. 4).

Two cases with respect to the oxidation states of the manganese ions were taken into account: first, the experimentally manifested $Mn^{II}$–$Mn^{III}$ situation; and, second, hypothetical $Mn^{II}$–$Mn^{IV}$ cluster. In the first case, the three-dimensional network has to have vacancies of $Mn^{III}(CN)_6$ units in order to result in a neutral three-dimensional network compound [14], which leads to the experimental formula $Mn_3[Mn(CN)_6]_2 \cdot 15\ H_2O$. The $[Mn_2(CN)_{11}]^{z-}$ unit is, on the one hand, five times negatively charged and, on the other hand, six times negatively charged. The second case shows the ideal stoichiometry for a neutral cubic PB phase, which is $M_2(CN)_6$ (M = transition metal).

The input for these calculations was based on the symmetry $C_{4v}$. It turned out that the results of the DFT calculations confirmed our expectations from previous calculations but with quantitative information about the relative stabilities. Tables VI and VII summarize our results. The empty signs (∅) are place holders for configurations, where the mixing of the orbitals was too high and no plausible occupations of the MOs were obtained. For the cases labeled "not converged," it was not possible to reach convergence criteria, because the self-consistent field (SCF) convergence criteria were the same for all calculations, which were the default parameters of the ADF program.

### Case Study: $Mn^{(II)}$–$Mn^{(III)}$

Several configurations were taken into account, namely, the HS and LS configurations and the interchange of the oxidation states of the manganese cations. Table VI summarizes the total electronic energies of the possible configurations. The label HS–LS in the second column of the table indicates that the first manganese is in HS and the second one is in LS. The "$\alpha$–$\beta$" column gives the total number of $\alpha$ and $\beta$ spins of the clusters. The two possibili-

**TABLE V**

**The set of results for $[Mn(CN)_6]^{z-}$ complexes with bond lengths corresponding to geometry 2 (see Table I) and point charges in the ligand position (see Fig. 3).**

| | $[Mn(CN)_6]^{-4}$ $Mn^{II}$ ($d^5$) | | $[Mn(CN)_6]^{-3}$ $Mn^{III}$ ($d^4$) | | $[Mn(CN)_6]^{-2}$ $Mn^{IV}$ ($d^3$) |
|---|---|---|---|---|---|
| | HS | LS | HS | LS | |
| N-coordinated | −147.75 | **−149.79** | −145.71 | **−146.25** | −134.10 |
| C-coordinated | −150.40 | **−151.47** | −143.55 | **−144.39** | −136.01 |

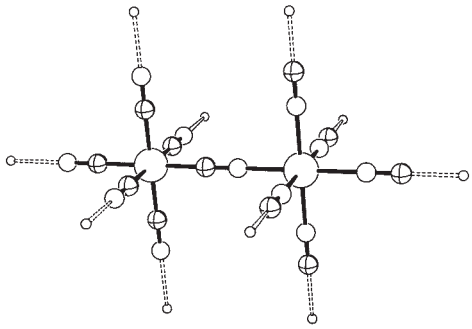

**FIGURE 4.** The dinuclear cluster with the cyanide bridging ligand; one manganese is C-coordinated and the second one is N-coordinated. We present also the positions of point charges adopted for this case and in agreement with the conclusion made on the study of the mononuclear compounds. We chose the ligand position for practical reasons.

ties for each case, therefore, correspond to an antiferromagnetic and to a ferromagnetic alignment of the spins of the two manganese ions, respectively, as indicated at the beginning of the second column by the labels "AF" (antiferromagnetic) and "F" (ferromagnetic).

It is notable that all energy values are comparable, because the total number of electrons is the same for each case. Clearly the table demonstrates that the two energies in the same block (antiferromagnetic and ferromagnetic) are quite close. But the energies in different cells differ significantly. In conclusion, the configuration with the $Mn^{II}$ in nitrogen coordination and the $Mn^{III}$ in carbon coordination is the favored one. In addition, the configurations with the $Mn^{III}$ in the LS state are more stable than the configurations in the HS state. Moreover, the influence of the change of the spin state of the $Mn^{III}$ is slightly bigger than that for the $Mn^{II}$ ion.

### Case Study $Mn^{(II)}$–$Mn^{(IV)}$

The same set of calculations was performed for the $Mn^{II}$–$Mn^{IV}$ unit, resulting in a charge of $z = -5$. The number of calculations is reduced by a factor of two, because for $Mn^{IV}$ ($d^3$) there is no HS or LS configuration. Table VII summarizes the results of the calculations. Because this case exhibits a different number of electrons than the previous one, it is not possible to compare the energies of the corresponding tables. Nevertheless, the same conclusions as above can be drawn: (1) the more stable configuration is with the manganese in the lower oxidation state linked to the nitrogen; (2) the manganese in nitrogen coordination is more stable in the HS state, and (3) the difference in energy between the two possible total spins is not very large.

## NEAR-IR SPECTRA

Figure 5 shows the near-IR spectrum of a single crystal of $Mn_3[Mn(CN)_6]_2 \cdot 15\ H_2O$ with a thickness of around 200 $\mu$m. The peaks located at 9200 $cm^{-1}$

**TABLE VI**

**The dinuclear cluster calculation for the case: $Mn^{(II)}$ –$Mn^{(III)}$ with energy expressed in [eV].**[a]

| Configuration | $\alpha$–$\beta$ | $Mn^{II}$ linked to N & $Mn^{III}$ linked to C | $Mn^{II}$ linked to C & $Mn^{III}$ linked to N |
|---|---|---|---|
| HS–LS[b] | AF[c] 6–3 | **−483.63** | −479.94 |
| | F 8–1 | −483.33 | Not converged |
| LS–LS | AF 4–5 | −481.58 | Not converged |
| | F 6–3 | −482.052 | Not converged |
| LS–HS | AF 3–6 | −478.40 | −473.28 |
| | F 7–2 | −479.58 | −470.77 |
| HS–HS | AF 5–4 | ∅ | −476.29 |
| | F 9–0 | −478.91 | −476.58 |

[a] For some calculations, we were unable to reach the convergences criteria (probably because in these cases, we tried to fix occupation too far from what is reasonable). For one case (empty sign one), the MO's are too mixed and we were not able to affirm that the calculation performed corresponds to the desired occupation.

[b] HS–LS means the first manganese (referring to the first row), of which $Mn^{II}$ is HS (high spin), and the second manganese, of which $Mn^{III}$ is LS (low spin). The C or N coordination change from column three to column four.

[c] Abbreviations: AF, antiferromagnetic interaction; F, ferromagnetic interaction.

**TABLE VII**
**The dinuclear cluster calculation for the case: $Mn^{(II)}$–$Mn^{(IV)}$.[d]**

| Configuration | $\alpha$–$\beta$ | $Mn^{II}$ linked to N & $Mn^{IV}$ linked to C | $Mn^{II}$ linked to C & $Mn^{IV}$ linked to N |
|---|---|---|---|
| HS[b] | AF 5–3 | −444.37 | −432.42 |
| | F 8–0 | −444.54 | ∅ |
| LS | AF 3–5 | Not converged | −433.90 |
| | F 6–2 | −444.12 | Not converged |

[a] The same convention is used for this table as in Table VI.
[b] For this case, we have to specify only the configuration of $d^5$ ($Mn^{II}$) because, for $d^3$, we cannot distinguish between HS and LS configuration.

could be assigned to the $^3T_1$ ($t_2^4$) → $^1T_2$ ($t_2^4$) transition of the $Mn^{3+}$ ions. The assignment was done on the basis of the absorption spectrum of the corresponding $K_3[Mn^{III}(CN)_6]$ sample as reference compound, also shown in Figure 5. The intensity of the absorptions of the $Mn_3[Mn^{III}(CN)_6]_2 \cdot 15\ H_2O$ is about 100 times larger than that of the reference sample $K_3[Mn^{III}(CN)_6]$, which could be due to the exchange interaction as a result of the bridging mode of the cyanide ligands. We decided to model this transition by ligand field (LF)-DFT theory [18, 19]. For this purpose, we studied the LF of $[Mn(CN)_6]^{-3}$ (Mn with an oxidation state of III: $d^4$). The procedure has three steps: (i) perform an average of configuration (AOC) calculation (put 0.4 electrons in each spin orbits of d-atomic orbitals) in order to optimize the Kohn–Sham orbitals, (ii) calculate the energy of all the Slater determinants (SDs) (210 for four electrons on 10 spin-orbits), and (iii) apply the procedure explained by Atanasov and al. [18, 19]. The complex was already studied in a previous work [19], although it had slightly different bond lengths (the difference is about 0.02 Å, and we consider the influence as negligible), and the Racah's parameters and ligand-field strength found were: $B = 630\ cm^{-1}$; $C = 2598\ cm^{-1}$; and $\Delta = 36900\ cm^{-1}$.

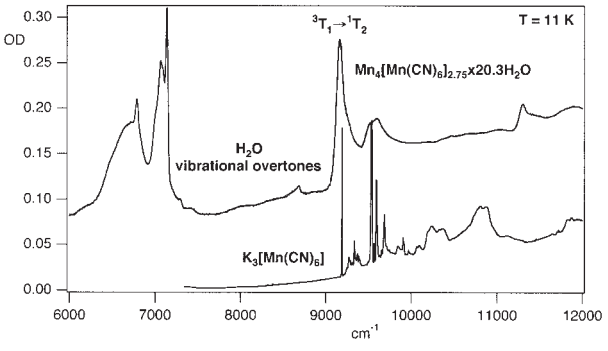


**FIGURE 5.** Near-IR spectra of a single crystal of the Mn–PB analogue with a thickness of 200 $\mu$m.

The full LF multiplet structure using classical LF theory can thus be determined. The predicted and observed values for the excitations considered are: $E(^3T_1 \rightarrow {}^1T_2)_{obs} = 9200\ cm^{-1}$; and $E(^3T_1 \rightarrow {}^1T_2)_{pred} = 7948\ cm^{-1}$.

From the results of these investigations, that is, spectroscopical and theoretical, we can conclude that the $^3T_1 \rightarrow {}^1T_2$ transition corresponds to the band observed in the near-IR spectra.

## Perspective: Magnetics Properties

In addition, the compound studied has interesting magnetic properties. The energy values of ferromagnetic and antiferromagnetic interactions for $Mn^{(II)}$ *HS*–$Mn^{(III)}$ LS given in Table VI allow us to evaluate the coupling constant J. Investigations are in progress. The first results are in qualitative agreement with experimental data and predict an antiferromagnetic ground state (estimated value of J is negative). If we refer to the magnetic susceptibilities measured experimentally and apply the Van Vleck formula, we observe that J has a value of about $-6\ cm^{-1}$. In the future, a challenging investigation will quantitatively determine this value by DFT. We plan to carry on studies in this direction.

## Conclusion

The DFT calculations revealed results that are in line with chemical intuition. When faced by this kind of challenge, two approaches are feasible: (i) band structure calculation, and (ii) model cluster. In

this study, we took the second approach. The results obtained, namely, Mn linked to N is HS, Mn linked to C is LS, no influence of point charge positions, $Mn^{(II)}$ HS linked to N − $Mn^{(III)}$ LS linked to C pattern in the crystal and antiferromagnetic ground state are quite convincing. However, it would be interesting if in the future band structure or lattice dynamic could be carried out in order to complete our knowledge of PB analogues.

We regret that we were not able to perform a frequency calculation of the dinuclear cluster due to technical problems, which will be solved in the future. These could then be directly compared with available experimental data.

### ACKNOWLEDGMENT

This work was supported by the Swiss National Science Foundation (grant number NRP47).

## References

1. Anonymous. Miscellenea Berolinensia ad Incrementum Scientiarum; Berlin, 1710, 1, 377.
2. Buser, H. J.; Ludi, A.; Petter, W.; Schwarzenbach, D. J Chem Soc Chem Commun 1972, 1299.
3. Ferlay, S.; Mallah, T.; Ouahès, R.; Veillet, P.; Verdaguer, M. Nature 1995, 378, 701.
4. Kahn, O. Nature 1995, 378, 667.
5. Holmes, S. M.; Girolami, G. S. J Am Chem Soc 1999, 121, 5593.
6. Sato, O.; Iyoda, T.; Fujishima, A.; Hashimoto, K. Science 1996, 272, 49.
7. Sato, O.; Iyoda, T.; Fujishima, A.; Hashimoto, K. Science 1996, 272, 704.
8. Te Velde, G.; Bickelhaupt, F. M.; Baerends, E. J.; Fonseca Guerra, C.; Van Gisbergen, S. J. A.; Snijders, J. G.; Ziegler, T. J Comput Chem 2001, 22, 931.
9. Slater, J. C. Quantum Theory of Molecules and Solids, Volume 4: Self Consistent Field for Molecules and Solids; McGraw-Hill: New York, 1974.
10. Vosko, S. H.; Wilk, L.; Nusair, M. Can J Phys 1980, 58, 1200.
11. Perdew, J. P.; Chevary, J. A.; Vosko, S. H.; Jackson, K. A.; Pederson, M. R.; Singh, D. J.; Fiolhais, C. Phys Rev 1992, B46, 6671.
12. Boerrigter, P. M.; Te Velde, G.; Baerends, E. J Int J Quantum Chem 1988, 33, 87.
13. Te Velde, G.; Baerends, E. J. J Comput Phys 1992, 99(1), 84.
14. Ludi, A.; Güdel, H. U. Struct Bonding 1973, 14, 1.
15. Pulay, P. Theor Chim Acta 1979, 50, 299.
16. Pulay, P. Chem Phys Lett 1980, 73, 393.
17. Hamilton, T. P.; Pulay, P. J Chem Phys 1986, 84, 5728.
18. Atanasov, M.; Daul, C. A.; Rauzy, C. Chem Phys Lett 2003, 367, 737.
19. Atanasov, M.; Daul, C. A.; Rauzy, C. Struc Bond 2004, 106, 97.
20. Mukherjee, R. K.; Chowdhury, M. Chem Phys Lett 1975, 34(1), 178.